RZ 1060 (#38164) 3/2/81
Communications/Computer Science/Engineering Technology 46 pages

Research Report

MECCA - A MULTIPLE-ERROR CORRECTION COMPUTATION ALGORITHM FOR BI-LEVEL IMAGE HARDCOPY REPRODUCTION

P. Stucki

IBM Zurich Research Laboratory, 8803 Rueschlikon, Switzerland

IBM Research Division
San Jose · Yorktown · Zurich

Copies may be requested from:

IBM Thomas J. Watson Research Center
Distribution Services 38-066
Post Office Box 218
Yorktown Heights, New York 10598

RZ 1060 (#38164) 3/2/81
Communications/Computer Science/Engineering Technology 46 pages

MECCA - A MULTIPLE-ERROR CORRECTION COMPUTATION ALGORITHM FOR BI-LEVEL IMAGE HARDCOPY REPRODUCTION

P. Stucki

IBM Zurich Research Laboratory, 8803 Rueschlikon, Switzerland

ABSTRACT: The properties of conventional, ordered dot-pattern generation techniques for bi-level halftone representation are examined and compared with the properties of error-diffusion based, disordered dot-pattern generation algorithms. The various processing steps necessary for the adaptation of the disordered halftone pattern-generation technique to digital image hardcopy reproduction with non-ideal computer-output printing devices are described. It includes procedures for spatial distribution of thresholding errors, suppression of dot-density artifacts and compensation for dot overlap. These procedures represent the core of the Multiple-Error Correction Computation Algorithm called MECCA, the objective of which is to linearize the non-ideal printing process in order to minimize the loss or shift of tonal gradations. Finally, the performance of MECCA is compared with a conventional digital screening technique and the various reproduction-quality versus computational-complexity trade-offs are discussed.

Februray 6, 1981

INTRODUCTION

The current trend in computer industry is towards computers that are smaller, faster and cheaper. The most important impetus for this increase in computer power has come from the improved performance of Large Scale Integration (LSI) electronic circuitry which has brought switching speed into the pico-second range. Very Large Scale Integration (VLSI) technology with its capability to further reduce the cost of storage and computing will strongly impact the speed and scope of the evolution from today's data-processing equipment to the information-processing systems of the future.

Today, the field of conventional data processing and data transmission is well established. While text processing and electronic document distribution have already been introduced, image and voice acquisition, processing, storage and retrieval are still in their infancy. However, here too, new technology is on the way to help. Advanced generations of computers and progress in the area of I/O devices will allow the remote copying of facsimiles, the storage and retrieval of financial, legal and technical documents, the handling of speech files, etc.

As more and more text-processing systems are able to cope with the arrangement of text within a page, attention shifts to the problem of digital preparation of artwork and illustrative material so that it can be composed along with text. The convenience of giving editors not only the option of placing a picture in its correct position, but also cropping, sizing and altering the photographic quality of these pictures, maximizes the amount of editorial control over the final product. Thus, the intent of such a publishing system is not only to set artwork and illustrative material, but also to process, store and retrieve them upon demand.

Artwork and illustrative material generally consists of logotypes, line-art and photographs. Their reproduction with an all-point-addressable computer-output printer requires them to be in bi-level form since printing processes generally exhibit only two levels of optical density: The presence or absence of ink or toner particles, for example. While the transformation of logotypes and line-art into bi-level form consists of a straightforward thresholding operation, the conversion of an analog continuous-tone image into a sampled bi-level halftone representation has motivated a number of research efforts.

The purpose of this paper is to describe an improved method to generate and manipulate bi-level halftone representations for high-resolution achromatic image rendition.

CONVERSION OF A CONTINUOUS-TONE IMAGE INTO A BI-LEVEL HALFTONE REPRESENTATION

General

For the conversion of a continuous-tone image into a bi-level halftone representation, a photograph or a natural scene is first scanned using a Charge-Coupled Device (CCD) or a video camera, for example. The resulting analog signal is then translated into digital form by sampling and amplitude quantizing the different shades of gray, ranging from all white to all black. The resolution of the digitized continuous-tone image is a function of the number of lines scanned N, the number of discrete samples or picture elements (pel) taken M, and the number of signal amplitude levels quantized Q.

A straightforward approach to convert a continuous-tone image into a bi-level halftone representation is to simulate the process of halftone photography. The latter is used in lithography and photoengraving and in principle, works as follows: When a halftone negative is made from a continuous-tone copy, a halftone screen - in the case of a contact screen an out-of-focus pattern of different dots and corresponding spaces - is placed in the light path between the camera lens and a sheet of high-contrast photographic film. The basic function of the halftone screen and the high-contrast photographic film is to convert the intermediate tones of the original continuous-tone copy into solid dots of equal density but varying size, the centers of which are placed on a regular grid.

Digital Halftone Photography

In digital halftone photography, the function of screening is achieved by comparing at each picture element position x, the scanned and digitized continuous-tone signal q(x) against a variable level, over i pels repetitive, threshold or dither pattern t[mod(x,i)], in order to make a black or white decision h(x) [1,2]. Figure 1 shows the principle of variable-level thresholding in one dimension. Corresponding examples of bi-level representations are shown in Figure 2.

In order to break-up the width-modulated vertical line structure originating from variable-level thresholding in one dimension, the continuous-tone signal q(x) has to be compared at each picture-element position x against a variable threshold profile that varies in the two image dimensions x and y (Figure 3).

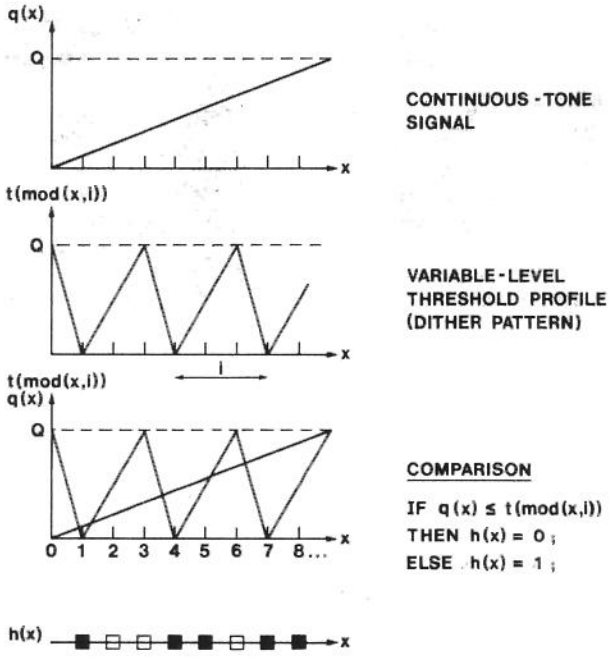

Figure 1. Principle of variable-level thresholding.

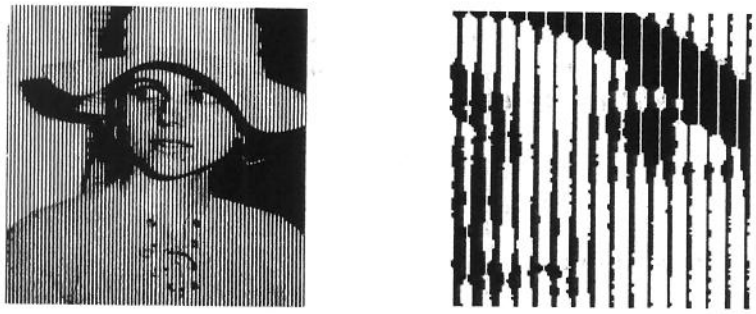

a) b)

Figure 2. One-dimensional variable-level thresholding.

a) Portrait picture
N=600 lines, M=600 pel.
b) Cropped and magnified eye portion of portrait picture
N=600 lines, M=600 pel.

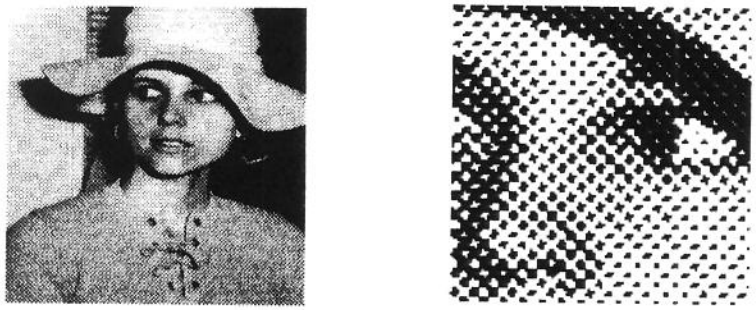

a) b)

Figure 3. Two-dimensional variable-level thresholding.

a) Portrait picture
N=600 lines, M=600 pel.
b) Cropped and magnified eye portion of portrait picture
N=600 lines, M=600 pel.

In practice, the digitized continuous-tone signal q(x,y) is compared against a two-dimensional, variable-level, over i and j repetitive threshold or dither pattern t[mod(x,i), mod(y,j)], to generate a bi-level halftone representation h(x,y), such that for q(x,y) = t[mod(x,i), mod(y,j)], h(x,y) = '0' (white) and '1' (black) otherwise. Because of the repetitive nature of the threshold profile t[mod(x,i), mod(y,j)] used, this screening method leads to a so-called *ordered dot pattern bi-level halftone representation.*

Threshold Profile Optimization

The penalty paid for the improved halftone rendition by two-dimensional variable-level thresholding is a certain loss of spatial resolution or pictorial detail. Over the past years, several design approaches to optimize the threshold profile with respect to spatial resolution and tonal fidelity have been proposed [3,4]. Typically, an optimized threshold profile for best possible spatial resolution rendition consists of a set of threshold values as shown in Figure 4a.

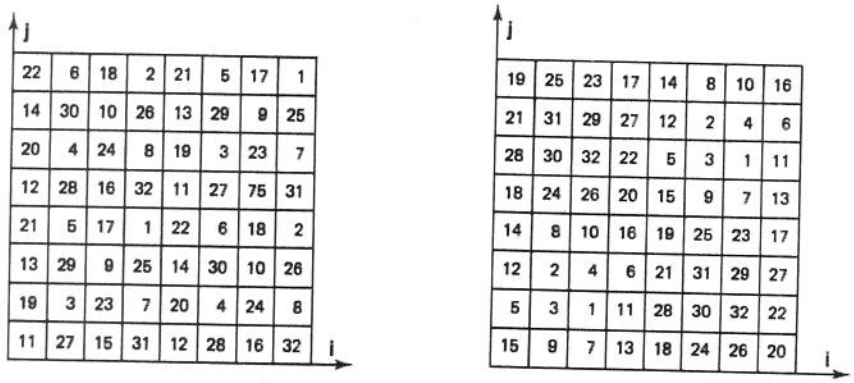

a) b)

Figure 4. Optimized threshold profiles t(i,j) for Q=32 amplitude quantization levels with respect to

a) spatial resolution; b) tonal fidelity.

This arrangement of threshold values can be characterized as one in which the t(i,j)th and the t(i,j)+1th threshold values are spatially located as far as possible away from one another in the threshold profile. Digital screens fulfilling this characteristic generate *dispersed dot patterns* having the capability of reproducing high spatial resolution at a linear dot-area-coverage versus amplitude-level relationship when reproduced with an ideal, i.e., square dot, on/off printing device. However, when using a non-ideal, i.e., circular dot, on/off printing device producing overlapping dots, as it occurs in non-impact ink-jet or electrophotographic printing, the dot-area-coverage versus amplitude relationship becomes dot-pattern dependent, i.e., non-linear and therefore, difficult to control without losing tonal fidelity.

A natural way to reduce the darkening effect of dot overlap is to generate *clustered dot patterns*. Typically, an optimized threshold profile for best-possible tonal-fidelity rendition consists of a set of threshold values as shown in Figure 4b. In this case, the threshold profile can be characterized as one in which the t(i,j)th and the t(i,j)+1th threshold values are spatially arranged as close as possible to one another, and where the clustered dot patterns run under 45^{o} and 135^{o}, respectively, an angle at which the cut-off

bandwidth for binocular vision is reduced by approximately 10 % as compared to horizontally and vertically oriented gratings [5]. Dot overlap is naturally compensated at the interior of the dot clusters and a close-to-linear dot-area-coverage versus amplitude-level relationship is achieved at the expense of a certain loss in spatial resolution. An analytic procedure to design clustered dot patterns based on the concept of SUPER-CIRCLES, or dot clusters with envelope of the general form

$$x^{2k} + y^{2k} = r^{2k},$$

$$\text{where} \quad 1 \leq k \leq \infty,$$

is described in [6].

The Rendition of Scanned Logotypes, Line-Art and Photographs

Artwork and illustrative material to be processed consists of logotypes, line-art and photographs or a combination of these. It is essential that the reproduction device be capable of rendering these different type of images with adequate quality. Logotypes and line-art can be characterized by sharp boundaries and the scanned and digitized continuous-tone signal $q(x,y)$ contains fast transients. Its proper rendition calls for high spatial-resolution requirements while a moderate number of amplitude quantization levels is sufficient to guarantee adequate reproduction quality. Photographs are quite different from logotypes and line-art. In areas with slowly varying gray-levels, the issue of tonal fidelity is very important and fine amplitude quantization is required, otherwise contouring will appear. At the same time, moderate spatial-resolution requirements usually guarantee adequate rendition quality.

A method to improve the digital bi-level representation whenever logotypes, art-work and photographs are intermixed consists of computing the Laplace gradient Δ at every picture element position (x,y) of the digitized continuous-tone signal $q(x,y)$ and adaptively switching between two different, two-dimensional threshold profiles. For example, if a fast transient is detected, $q(x,y)$ will be compared with a threshold profile generating dispersed dot patterns, otherwise the threshold profile rendering clustered dot patterns will be used [7]. The concept of adaptive switching of dispersed and clustered dot patterns for bi-level halftone representation removes, to a certain extent, the spatial-resolution and tonal-fidelity restrictions encountered in conventional screening.

Multiple-Copying of Bi-Level Halftone Representations

The various bi-level halftone representation techniques discussed so far have been evaluated in terms of their multiple digital copying potential and as a function of different scanning-aperture and light-collector device characteristics. The investigation is based on an extended simulation to model the various steps involved in the entire halftone document copying cycle, starting off from a digitized continuous-tone signal q(x,y) ready for conversion into its first bi-level halftone representation h(x,y), followed by a re-scanning process performed under arbitrary tilt angle α to obtain a new digitized continuous-tone signal q'(x,y) ready for a second, not necessarily the same conversion into a new bi-level halftone representation h'(x,y), etc.

Figure 5. Re-scanning bi-level halftone representations.

Clustered dot pattern re-scanned with a) a rectangular-shaped aperture profile; b) a Gaussian-shaped aperture profile.

Figure 5a shows a clustered dot pattern bi-level halftone representation originally printed at a resolution of 400 pel/inch and re-scanned at a resolution of 480 pel/inch, a tilt angle of $\alpha = 1.5^{o}$ and assuming a square aperture profile, which is found typical for CCD's. The same picture re-scanned under the same condition, but assuming a Gaussian aperture profile as encountered in laser scanners is shown in Figure 5b. The Moire pattern formation observed in Figures 5a and b are a direct function of the generating dot-pattern structure, the tilt angle α and the shape of the aperture profile. A possible way to suppress the formation of such interferences is to enlarge the scanning aperture beyond the screening resolution of the original picture. However, such a filtering approach degrades the sharpness of the re-scanned picture. Figures 6a, and b show the result of Moire-free re-scanning using an enlarged Gaussian aperture profile.

Figure 6. Moire-free re-scanning using an enlarged Gaussian aperture profile.

Re-scanning with a) 8 pel x 8 pel aperture;
b) 12 pel x 12 pel aperture.

Pseudo-Random Thresholding

An alternative way to suppress the formation of Moire patterns is to use pseudo-random thresholding techniques to generate bi-level representations of halftones. In this case, the digitized continuous-tone signal q(x,y) is compared, at each pel position (x,y), with a pseudo-random threshold signal t(x,y) to generate h(x,y) such that for $q(x,y) \leqq t(x,y)$, h(x,y) = '0' (white) and '1' (black) otherwise. Because of the pseudo-random nature of the threshold signal t(x,y), this screening method leads to a so-called *disordered dot pattern bi-level halftone representation* (Figure 7).

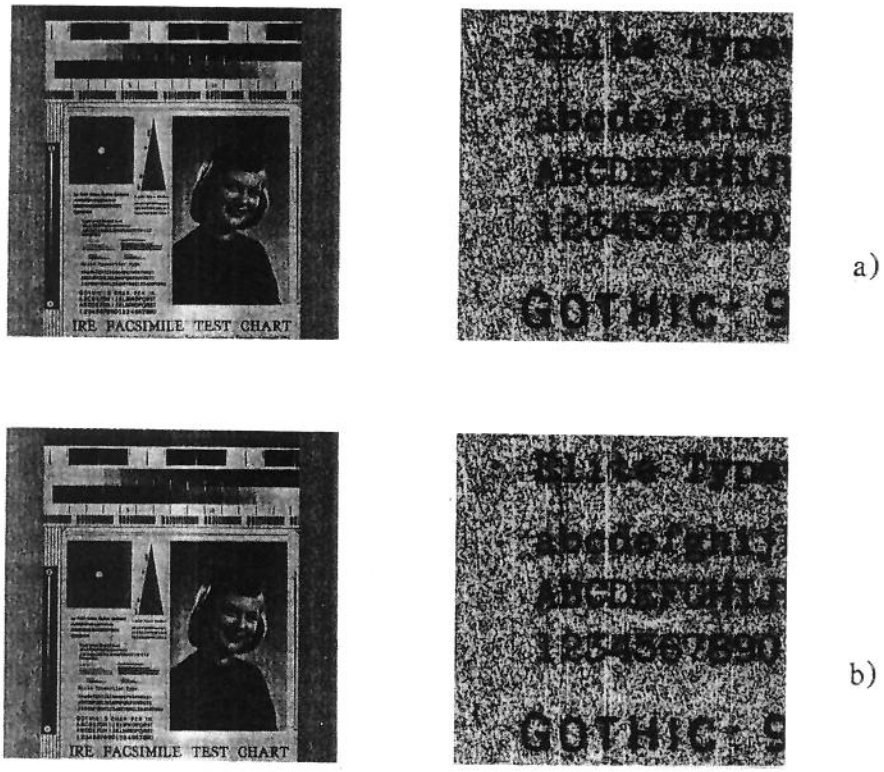

a)

b)

Figure 7. Pseudo-random thresholding to generate bi-level representations of halftones.

a) Original; b) re-scanned with 8 x 8 Gaussian aperture.

It is interesting to note that no Moire pattern formation takes place when re-scanning and subsequent pseudo-random thresholding a bi-level representation originally generated with pseudo-random thresholding halftone techniques (Figure 7b). Unfortunately, the actual appearance of the picture quality obtained is rather poor. An explanation for the shortcoming of this approach is the fact that the pseudo-random threshold signal t(x,y) has a uniform spectral density distribution, i.e., it contains equally strong spectral components at all spatial frequencies which add-up to the spectral density distribution proper to the pictorial information in the visible as well as in the invisible frequency range. Pseudo-random thresholding can be classified as a *stochastic, non-linear process* capable of transforming a digitized continuous-tone signal q(x,y) into a disordered pattern bi-level halftone representation.

Fixed-Level Thresholding and Error Diffusion

In order to avoid the undesired uniform spectral density distribution characteristics of pseudo-random thresholding, a *deterministic, non-linear process* leading to a disordered dot pattern bi-level halftone representation is based on constant-level thresholding and error-carry (Figure 8).

Its principle of operation in one dimension is as follows: At every picture-element location x, a corrected digital continuous-tone value q'(x), representing the sum of the digitized continuous-tone signal q(x) and a carried error value e(x-1) arising from processing the previous neighbor pel, is compared with a spatially-independent constant-level threshold t(x) set at Q/2,to generate a bi-level halftone representation h(x) such that for $q'(x) = q(x) + e(x-1) \leqq Q/2$, h(x) = '0' (white) and 'Q' (black) otherwise.

A straightforward one-dimensional error-carry approach tends to generate subjectively disturbing line texture and in practice, the error value e(x) is distributed amongst the surrounding neighbors. This two-dimensional process is called error-diffusion. It requires more processing power and buffer memory than the error-carry approach but has the advantage of removing to a large extent the spatial-resolution and tonal-fidelity restrictions encountered in ordered pattern halftone generation. There exist basically two different strategies to achieve error-diffusion in two dimensions. In a first approach, fractions of the error-value e(x,y) at each picture-element position (x,y), are apportioned to the neighborhood digitized continuous-tone signal values still to be thresholded [8]. In a second approach, a weighted average of previously determined neighborhood error-values is added to the continuous-tone signal value q(x,y) at picture-element position (x,y), ready for thresholding [9]. This second approach is called minimized average error algorithm and was developed to display continuous-tone pictures on gas-discharge displays.

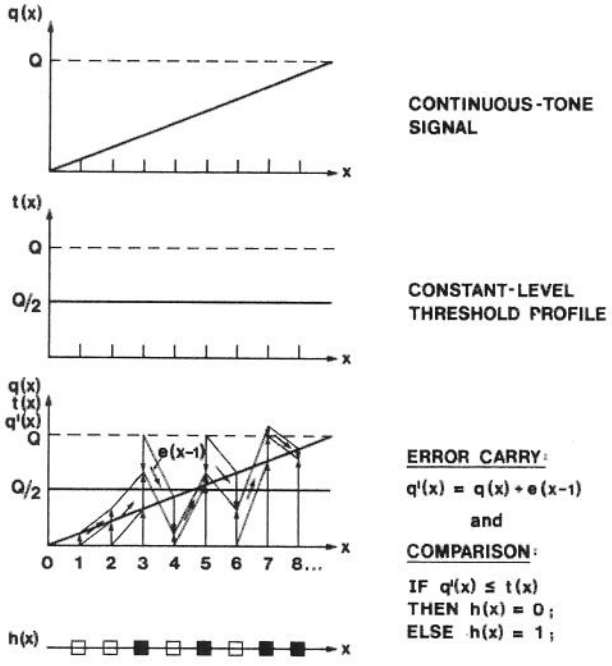

Figure 8. Principle of constant-level thresholding and error-carry.

The purpose of this paper is to describe how to enhance the latter concept of error diffusion to generate pseudo-disordered dot patterns for bi-level halftone representation and how to adapt this technique for *achromatic hard-copy reproduction with non-ideal printing devices.*

PSEUDO-DISORDERED DOT-PATTERN GENERATION FOR BI-LEVEL HALFTONE HARDCOPY REPRODUCTION

Constant-Level Thresholding and Two-Dimensional Error-Diffusion

The principle of constant-level thresholding and two-dimensional error-diffusion is shown in Figure 9.

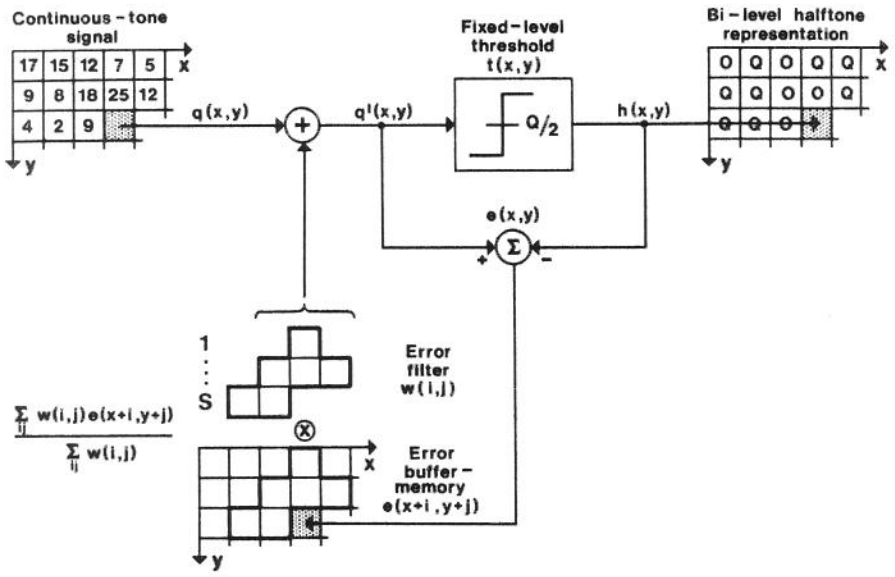

Figure 9. Principle of constant-level thresholding and two-dimensional error-diffusion.

At each picture-element position (x,y), a corrected digital continuous-tone signal q'(x,y), representing the sum of the digital continuous-tone signal q(x,y) and a weighted average of previously computed errors, is first calculated:

$$q'(x,y) = q(x,y) + \sum_{i,j} (w(i,j)\ e(x+i,y+j)) \ / \ \sum_{i,j} w(i,j),$$

where $w(i,j)$: error-filter impulse response extending over (i,j),
$e(x+i,y+j)$: error value at (x+i,y+j).

The corrected digital continuous-tone signal q'(x,y) is then compared with a fixed-level threshold t(x,y) set at Q/2 to generate a halftone representation h(x,y) such that for $q'(x,y) \leqq Q/2$, h(x,y) = '0' (white) and 'Q' (black) otherwise. Although the outcome of this non-linear operation is either '0' or 'Q', the actual density of the digitized continuous-tone signal q(x,y) can be anywhere in between. To complete the computation cycle, the thresholding error $e(x,y) = q'(x,y) - h(x,y)$ is determined and loaded into an S x M wide error buffer-memory for subsequent use in the following thresholding cycles. Constant-level thresholding and two-dimensional error-diffusion for the computation of intermediate average densities proceeds from left to right and from top to bottom in the N x M array.

Filter Optimization

Constant-level thresholding and two-dimensional error-diffusion produces a deterministic arrangement of disordered dot patterns. The 'degree of disorder' is determined by the characteristics of the error-filter used. In order to determine the optimum filter size and filter coefficients, three different error-filters with impulse responses shown in Figure 10 were studied.

```
1       2          1   1 2 4 2 1          1   2 2 2 2 2 2 2
.     2 8 2        .   2 4 8 4 2          .   2 4 4 4 4 4 2
S   2 8 x          S   4 8 x              .   2 4 8 8 8 4 2
                                           S   2 4 8 x
```

a) b) c)

Figure 10. Impulse response coefficients w(i,j) of different-size error-filters.

a) 'Small' spatial extent (S=3).
b) 'Medium' spatial extent (S=3).
c) 'Large' spatial extent (S=4).

It should be noted that the values of all weight coefficients are chosen to be 2^k, where k = 0, 1, 2, 3, ... , in order to improve computational efficiency. The 'small' error-filter is capable of reproducing dark areas reasonably well. For the rendition of light areas, however, the 'degree of disorder' in the dot-placement structure is not satisfactory. Instead, their positions are correlated in such a way as to produce diagonal streaks in the bi-level halftone representation. The 'degree of disorder' can also be expressed in terms of a two-dimensional power-spectrum plot which clearly indicates a certain angular preference in the distribution of the individual dot-pattern frequency components (Figure 11a).

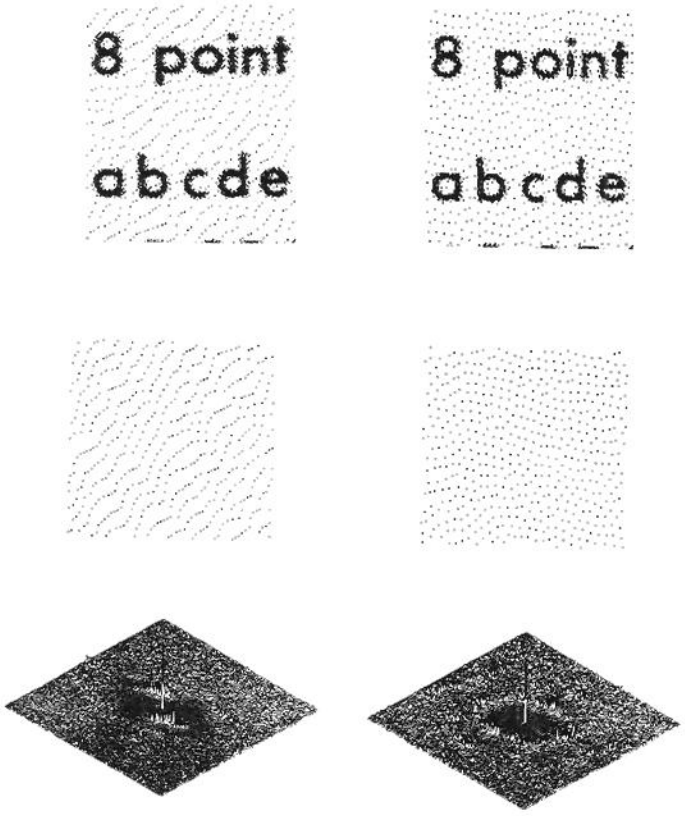

Figure 11. Error-filter size and 'degree of disorder'.

a) 'Small' spatial extent; b) 'medium' spatial extent.

It should be noted that these streaks correspond to the direction of maximum weighting in the error filter, i.e., the two eights run diagonally next to each other. Disturbing texture can be avoided - at the expense of computational efficiency - by increasing the spatial extent of the error-filter. The rendition of light areas is very much improved when using the 'medium' error-filter. In this case, the two-dimensional power-spectrum plot no longer indicates an angular preference, but shows a close to rotation-symmetric distribution of the individual dot-pattern frequency components (Figure 11b). Experiments using the 'large' error-filter indicate no substantial improvement in terms of dot-placement regularity.

Look-Ahead Fitering to Reduce Dot-Density Artifacts

Because of the finite spatial extent and the band-limiting characteristics of the impulse response w(i,j) of the error-filter, subjectively disturbing 'density overshoots' occur when reproducing high-contrast, large-area patterns (Figure 12).

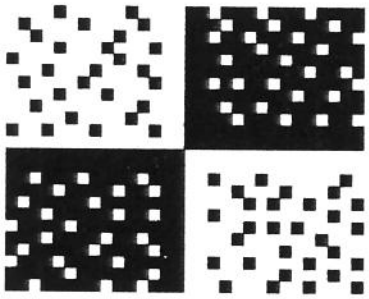

Figure 12. Example of 'density overshoot' in chequer-board pattern.

In order to suppress the formation of such artifacts, the constant-level thresholding and two-dimensional error-diffusion process has been complemented with a two-dimensional transient detection or look-ahead filter operating over a T x M wide input value buffer memory (Figure 13).

At each picture element position (x,y), the corrected digital continuous-tone signal q'(x,y) is now determined as a sum of the digital continuous-tone signal q(x,y), a weighted average of previously computed errors and, new, a term reflecting the local image texture:

$$q'(x,y) = q(x,y) + \sum_{i,j} (w(i,j)\ e(x+i,y+j)) \ / \ \sum_{i,j} w(i,j)$$

$$+ \sum_{i,j} (z(k,l)\ q(x+k,y+l)) \ / \ \sum_{i,j} z(k,l),$$

where $z(k,l)$: look-ahead filter impulse response extending over (k,l),
$q(x+k,y+l)$: amplitude value at (x+k,y+l).

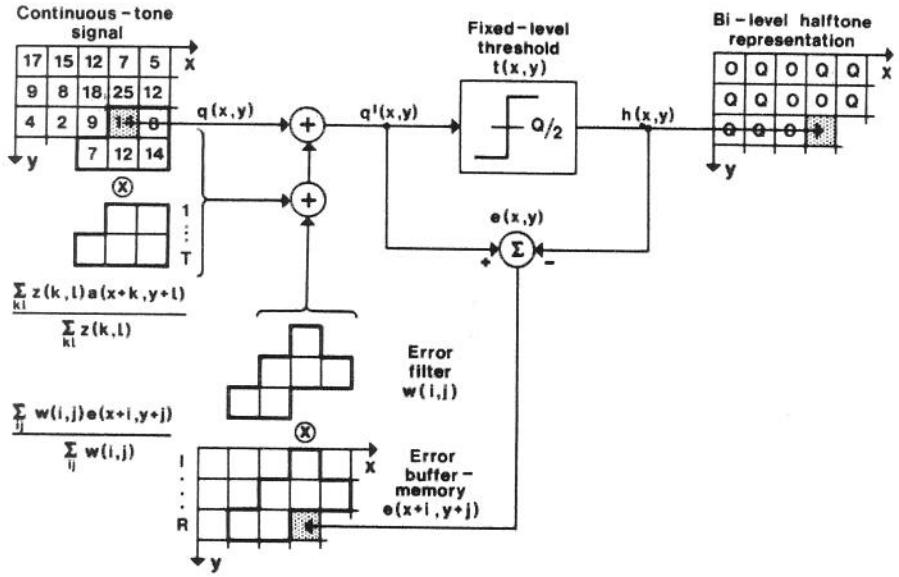

Figure 13. Principle of constant-level thresholding, two-dimensional error-diffusion and look-ahead filtering.

Like in the previous case, the corrected digital continuous-tone signal q'(x,y) is then compared with a fixed-level threshold t(x,y) set at Q/2 to generate a halftone representation h(x,y) such that for $q'(x,y) \geqq Q/2$,

h(x,y) = '0' (white) and 'Q' (black) otherwise. To complete the computation cycle, the error e(x,y) = q'(x,y) - h(x,y) is again determined and loaded into the S x M wide error buffer-memory for subsequent use in the following threshold cycles.

Several look-ahead filters have been investigated whereby the impulse response z(k,l) shown in Figure 14a represents a compromise. Together with a 'medium' error-filter, this look-ahead filter prevents the appearance of artifactual density overshoots when reproducing high-contrast, large-area patterns without noticeable blurring (Figure 14b).

$$\frac{1}{T}\begin{matrix} 16 & 2 \\ 1 & 2 & 1 \end{matrix}$$

a)

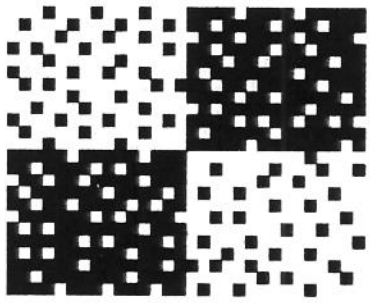

b)

Figure 14. Look-ahead filtering to prevent density overshoots.

a) Impulse response z(k,l).
b) Reproduced chequer-board pattern.

Dot-Size Correction to Compensate for Dot Overlap

The degree of perfection reached in constant-level thresholding, two-dimensional error-diffusion and look-ahead filtering is not yet sufficient to perform well for hardcopy reproduction with non-ideal printing devices.

In all-point-addressable computer-output printing, electrophotographic, ink-jet and other non-impact printing technologies are used. Square-shaped dots, as shown in the simulated chequer-board patterns of Figures 13 and 14a, cannot be printed with toner and ink-based recording technologies. Instead, individual dots are circular in shape when printed on ideal paper.

Given this technology limitation, the reproduction of continuous areas of black is only possible by causing adjacent dots to overlap (Figure 15a). In this case, however, the exact rendition of average densities becomes dependent on the combination of adjacent neighboring dots already printed and the resulting overdarkening has to be removed with a space-variant dot-size correction algorithm.

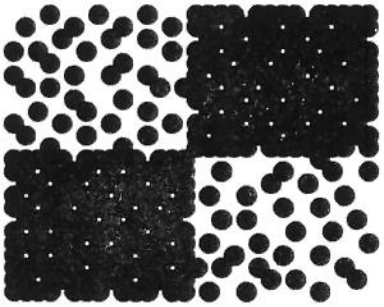

a)

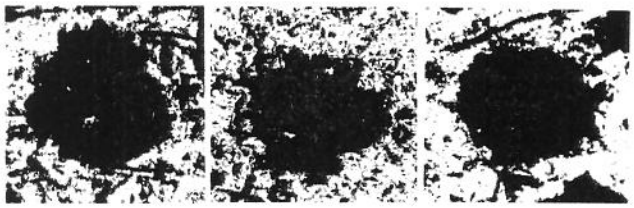

b)

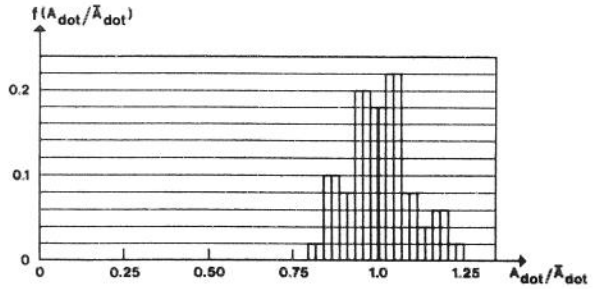

c)

Figure 15. Printing with circular-shaped dots.

a) Reproduced chequer-board (simulation).
b) Examples of dots printed on electro-sensitive paper.
c) Histogram of measured dot-size A_{dot}.

In practice, paper does not exist in ideal form, and fluctuations in dot shape as shown in Figure 15b are very likely to occur. Figure 15c shows the histogram of measured dot-size A_{dot}. It was determined by taking microscopic photographs of a set of dots and measuring their surface with a Polarplanimeter. Dot-placing experiments on normal and electro-sensitive paper have shown that the fluctuations in dot size and shape are stochastic and that they do not influence the overall average densities over larger dot-pattern areas. Thus, the analytic treatment of dot-size correction then consists in determining the area of white paper which a circular dot newly covers, when it is printed (Figure 16).

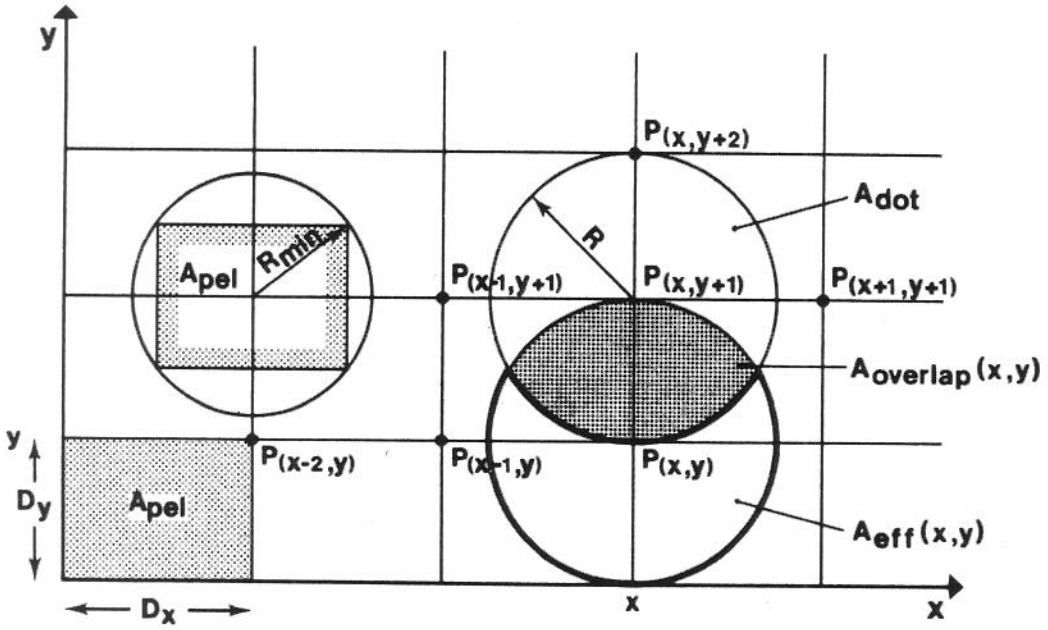

Figure 16. Parameters for dot-size correction.

P(x,y) denotes the dot center for the current print position. Previously printed dots may be located at P(x-1,y), P(x-2,y), ..., P(x+1,y+1), P(x,y+1), P(x-1,y+1), ..., P(x,y+2), ..., etc.. D_X and D_y represent the distance between adjacent print positions in x and y. The area of a picture element is defined as

$$A_{pel} = D_X D_y.$$

In order to guarantee the complete coverage of A_{pel} with a circular dot, its radius R must fulfill the condition

$$R \geq R_{min} = (\sqrt{D_x^2 + D_y^2})/2.$$

Area overlap amongst adjacent circular dots with radius R occurs for all

$$R > [\min(D_x, D_y)]/2.$$

Since

$$\sqrt{D_x^2 + D_y^2} > \min(D_x, D_y),$$

area overlap will always occur under the above condition of full pel coverage whenever adjacent dots are present.

If $A_{dot} = \pi R^2$ denotes the area of a dot without overlap and $A_{overlap}(x,y)$ the total area of overlap amongst adjacent dots, the effective area $A_{eff}(x,y)$ of white paper newly covered by a dot printed at P(x,y) amounts to

$$A_{eff}(x,y) = A_{dot} - A_{overlap}(x,y)$$

$$= \pi R^2 - A_{overlap}(x,y).$$

Finally, the dot-size correction value $\lambda(x,y)$ applying at print position P(x,y), is defined as

$$\lambda(x,y) = A_{eff}(x,y)/A_{pel}.$$

If L represents the number of adjacent print positions considered, $\lambda(x,y)$ can take any of 2^L values depending on the combinations of printed dots. Given D_X, D_y, R and L proper to an all-point-addressable computer-output printer, all 2^L possible dot-size-correction values $\lambda(x,y)$ have to be determined and stored in a device-specific look-up table.

A straightforward approach to compute $\lambda(x,y)$ is to use raster-graphic techniques (Figure 17).

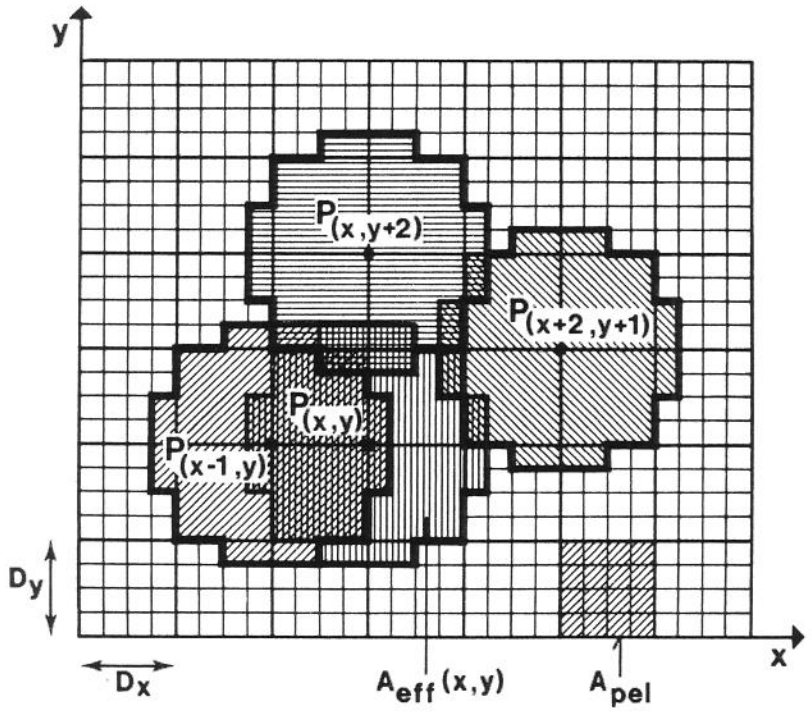

Figure 17. Raster-graphic approach to determine $A_{eff}(x,y)$.

For each of the 2^L possible dot-pattern combinations, digital approximations of printed circular dots are placed at relative print positions spaced D_x and D_y raster elements apart. Another digital approximation of a printed circular dot is then placed at P(x,y), and the number of newly covered 'white' raster elements, representing $A_{eff}(x,y)$, determined. For a worst-case $\lambda(x,y)$ accuracy of 1 %, A_{pel} should be represented by 10 x 10 raster elements or more.

The dot-size-correction factor $\lambda(x,y)$ can also be determined analytically. In order to fulfill the condition of covering A_{pel} with a circular dot, as well as to guarantee a unique dot-overlap order, the computation of $A_{overlap}(x,y)$ and consequently $\lambda(x,y)$ requires certain restrictions on the geometry and the values of D_x, D_y, R and L as outlined in the following two cases.

FIRST CASE (L=4)

In this case, dots printed at the four adjacent print positions P(x-1,y), P(x,y+1), P(x-1,y+1) and P(x+1,y+1) may contribute to area overlap when a new dot is printed at P(x,y).

Restrictions on D_x and D_y

The condition to guarantee a fixed dot-overlap order implies that the largest distance between P(x,y) and any of its L=4 neighbors

$$D_{max} = \sqrt{D_x^2 + D_y^2},$$

be less than the next larger distance between P(x,y) and any other print position possible

$$D_{next} = 2 \min(D_x, D_y).$$

Given this print-position geometry constraint, the restriction on the values of D_x and D_y can be expressed by

$$\max(D_x, D_y) \leq \sqrt{3} \min(D_x, D_y).$$

Restriction on R

In order to guarantee complete coverage of A_{pel} with a circular dot, as well as to exclude any overlay from all print positions other than the four adjacent neighbors, the range of R is determined by

$$(\sqrt{D_x^2 + D_y^2})/2 \leq R \leq \min(D_x, D_y).$$

Discussion

The selection of D_x, D_y and R within these boundaries allows the analytical computation of $\lambda(x,y)$. For $D_x = D_y = D$, the dot radius R can vary from 0.707D to D, while for $D_y = \sqrt{3} D_x$, it cannot assume any value other than D_x.

The determination of all possible 2^4 $A_{overlap}(x,y)$, $A_{eff}(x,y)$ and $\lambda(x,y)$ values when printing a new dot at P(x,y) is described in Appendix I.

SECOND CASE (L=6)

In this case, the four adjacent print positions P(x-1,y), P(x,y+1) P(x-1,y+1) and P(x+1,y+1) as well as the two next closest print positions P(x-2,y) and P(x,y+2) may contribute to area overlap when a new dot is printed in P(x,y).

Restrictions on D_x and D_y

The condition to guarantee a fixed dot-overlap order implies that the largest distance between P(x,y) and any of its L=6 neighbors

$$D_{max} = 2 \max(D_x, D_y),$$

be less than the next larger distance between P(x,y) and any other print position possible

$$D_{next} = \min(\sqrt{D_x^2 + 4D_y^2}, \sqrt{D_y^2 + 4D_x^2}).$$

Given this print-position geometry constraint, the restriction on the values of D_x and D_y can be expressed by

$$\max(D_x, D_y) \leq 2/\sqrt{3} \min(D_x, D_y).$$

Restriction on R

In order to guarantee complete coverage of A_{pel} with a circular dot, as well as to exclude any overlay from all print positions other than the six neighbors considered, the range of R is determined by

$$\max(D_x, D_y) \leq R \leq \min[(\sqrt{D_x^2 + 4D_y^2})/2, (\sqrt{D_y^2 + 4D_x^2})/2].$$

Discussion

The selection of D_x, D_y and R within these boundaries allows the analytical computation of $\lambda(x,y)$. For $D_x = D_y = D$, the dot radius R can vary from D to 1.11D, while for $D_y = 2/\sqrt{3} D_x$, it cannot assume any value other than D_y.

The determination of all possible 2^6 $A_{overlap}(x,y)$, $A_{eff}(x,y)$ and $\lambda(x,y)$ values when printing a new dot at P(x,y) is described in Appendix II.

Dot-Size Corrected Bi-Level Representation of Halftone

In order to guarantee an overlap or dot-size corrected bi-level representation of halftones, the corrected digital continuous-tone signal q'(x,y), determined as a sum of the digital continuous-tone signal q(x,y), a weighted average of previously computed errors and a term reflecting the local image texture, is first computed. The value of q'(x,y) is then compared with a fixed-level threshold t(x,y) set at Q/2 to generate a halftone representation h(x,y) such that for $q'(x,y) \geq Q/2$, h(x,y) = '0' (white) and 'Q' (black) otherwise. To complete the computation cycle, a new overlay and dot-size dependent error $e(x,y) = q'(x,y) - [\lambda(x,y)\ h(x,y)]$ is then determined and loaded into the S x M wide error buffer-memory for subsequent use in the following thresholding cycles.

The results obtained using a 'medium'-size error-filter w(i,j), the optimized look-ahead filter z(k,l) as well as dot-size correction parameters $D_X = D_Y = D$ and $R = 0.8D$ are shown in Figure 18.

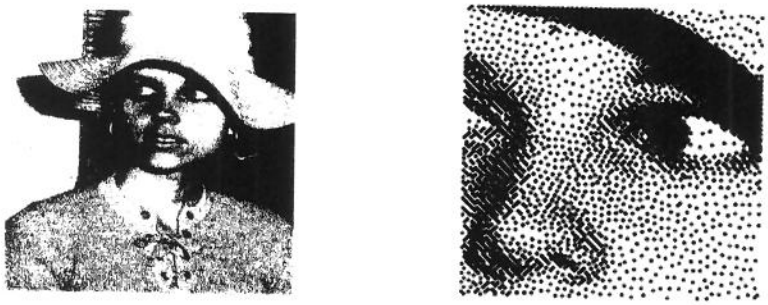

a) b)

Figure 18. Constant-level thresholding, two-dimensional error-diffusion, look-ahead filtering and dot-size correction.

a) Portrait picture
N=600 lines, M=600 pel.
b) Cropped and magnified eye portion of portrait picture
N=600 lines, M=600 pel.

For comparison, the same picture reproduced without dot-size correction is shown in Figure 19.

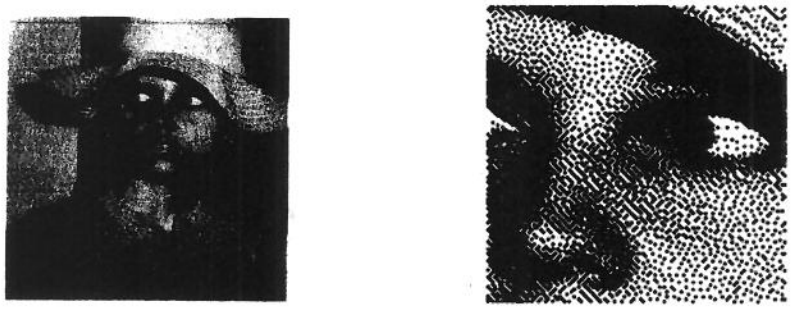

a) b)

Figure 19. Constant-level thresholding, two-dimensional error-diffusion and look-ahead filtering.

a) Portrait picture
N=600 lines, M=600 pel.
b) Cropped and magnified eye portion of portrait picture
N=600 lines, M=600 pel.

The area coverage c as a function of a synthetically generated amplitude quantization level q, varying over a range $0 < q < 127$, where '0' represents black and '127' white, is plotted in Figure 20. Curve a) corresponds to an 'open-loop' mode of the dot-size-correction scheme, i.e., the area coverage c is proportional to the newly covered area $A_{eff}(x,y)$ integrated over the entire range of g and without the dot-size-correction factor $\lambda(x,y)$ influencing the computation of the error-value e(x,y). Curve b) corresponds to a 'closed-loop' mode of the dot-size-correction scheme, i.e., the area

coverage c is proportional to $A_{eff}(x,y)$ integrated over the entire range of q and with $\lambda(x,y)$ being used for the computation of e(x,y). Working with exact values for D_x, D_y and R, the use of dot-size correction yields a linear correspondence between the area coverage c and the synthetically generated gray-value q.

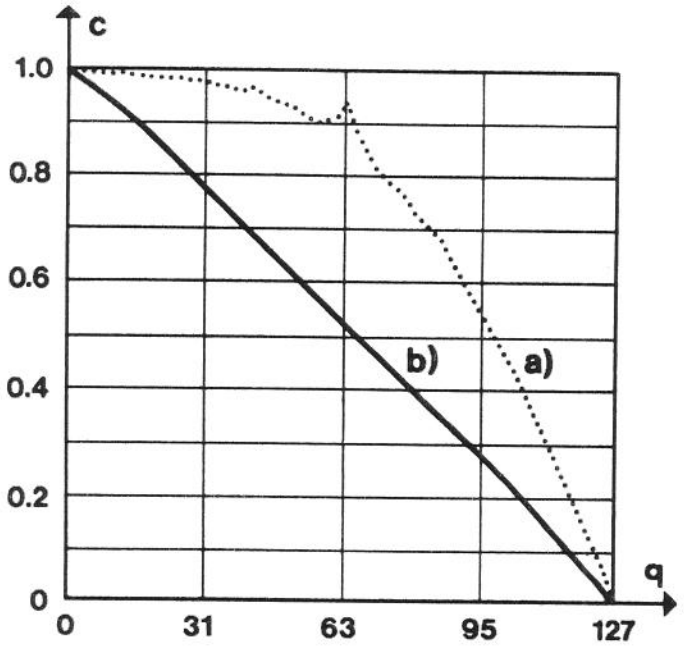

Figure 20. Area coverage c as a function of a synthetically generated amplitude quantization level q ('0' = black, '127' = white).

a) Without, b) with dot-size correction.

Several steps towards adapting the pseudo-disordered dot-pattern generation technique for bi-level halftone hardcopy reproduction have been discussed. They include procedures for spatial distribution of thresholding errors, the suppression of artifactual density overshoots and the compensation for dot overlap when using non-ideal computer-output printing devices. These procedures are all integrated into a single *Multiple-Error Correction Computation Algorithm called MECCA*.

DISCUSSION OF MECCA

Comparison with SUPER-CIRCLE Screening

The Multiple-Error Correction Computation Algorithm combines linear and non-linear signal-processing techniques to yield a bi-level halftone representation that is, on a minimized average basis, directly proportional to the continuous-tone input value. Linearizing a non-ideal printing process with MECCA minimizes the loss or shift of tonal gradations and therefore, guarantees best-possible halftone rendition for given printer characteristics.

To verify *qualitatively* the performance of MECCA and SUPER-CIRCLE screening techniques, typical examples of continuous-tone text, graphics and natural images were processed. The illustrations used in these experiments are cropped pictures from the IEEE Facsimile Test Chart, originally scanned at a spatial resolution of 200 pel/inch and quantized into Q=255 amplitude levels. Prior to the actual MECCA and SUPER-CIRCLE processing, the cropped pictures were scaled to 750 x 750 pels using two-dimensional third-order polynomial interpolation and resampling techniques [6].

Continuous-tone text (Figure 21)

Due to the high spatial-resolution rendition property of MECCA, continuous-tone text, where edge information is known to be visually important, is reproduced with well-defined contours and without noticeable screening artifacts. In contrast, the visibility of impaired contours which are due to the clustering of dots in SUPER-CIRCLE screening, makes the latter a bad choice for computer-output printing of continuous-tone text. A cropped and magnified letter 'A' out of Figure 21 is reproduced in Figure 22. It clearly shows the poor reproduction of edges obtained with SUPER-CIRCLE screening.

Continuous-tone graphics (Figure 23)

Due to the pseudo-disordered dot-pattern arrangement property of MECCA, continuous-tone graphics, where topological connectivity is known to be visually important, is reproduced with good definition and without noticeable screening artifacts. In contrast, the visibility of interferences or Moire patterns formed by the superposition of an ordered

Figure 21. Bi-level represenation of continuous-tone text.

a) MECCA, Q=256.
b) SUPER-CIRCLE, Q=32.
   Screening resolution: 70 clusters of dots/inch.
c) SUPER-CIRCLE, Q=64.
   Screening resolution: 47 clusters of dots/inch.
d) SUPER-CIRCLE, Q=128.
   Screening resolution: 35 clusters of dots/inch.

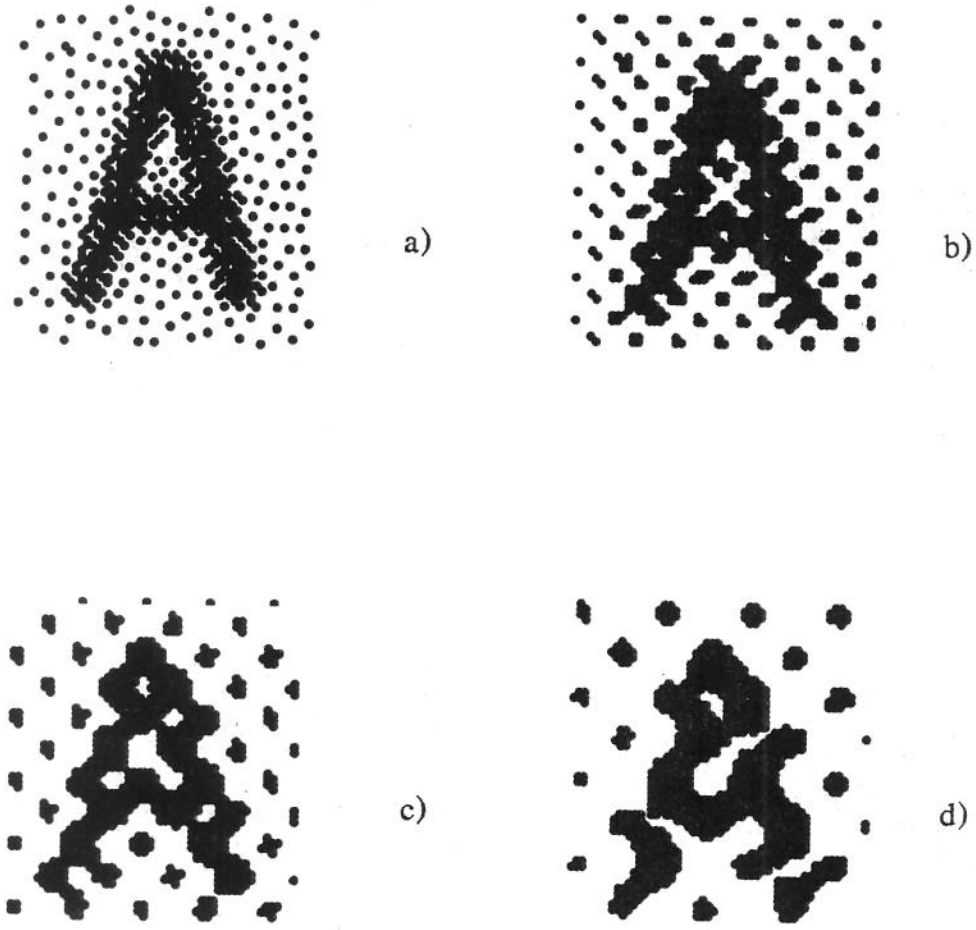

Figure 22. Cropped and magnified letter 'A'.

a) MECCA, Q=256.
b) SUPER-CIRCLE, Q=32.
   Screening resolution: 70 clusters of dots/inch.
c) SUPER-CIRCLE, Q=64.
   Screening resolution: 47 clusters of dots/inch.
d) SUPER-CIRCLE, Q=128.
   Screening resolution: 35 clusters of dots/inch.

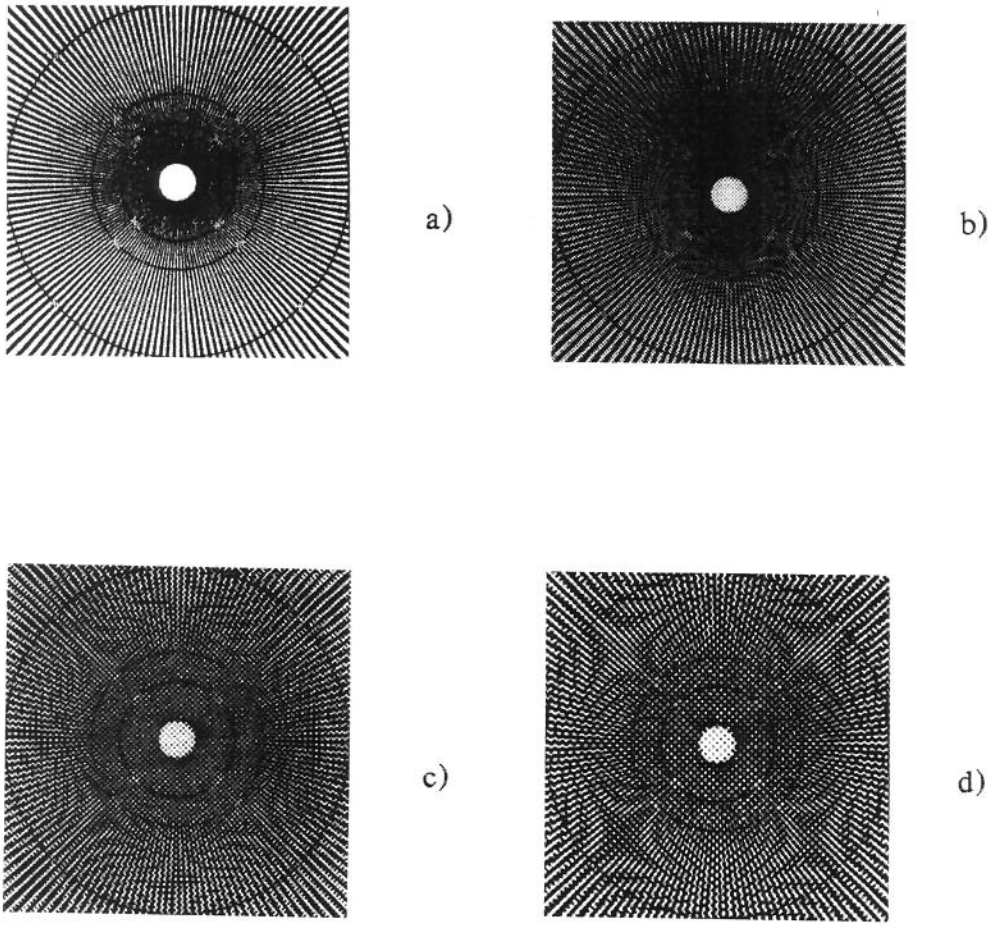

Figure 23. Bi-level representation of continuous-tone graphics.

a) MECCA, Q=256.
b) SUPER-CIRCLE, Q=32.
Screening resolution: 70 clusters of dots/inch.
c) SUPER-CIRCLE, Q=64.
Screening resolution: 47 clusters of dots/inch.
d) SUPER-CIRCLE, Q=128.
Screening resolution: 35 clusters of dots/inch.

graphic structure with an ordered dot-pattern texture as encountered in SUPER-CIRCLE halftoning, makes the latter a poor choice for computer-output printing of continuous-tone graphics. This experiment also demonstrated the higher-resolution rendition capability and the Moire-pattern formation inhibition property of MECCA, features which are of primary importance in all two-dimensional resampling tasks, i.e., scanning, interpolation, decimation, etc.

Continuous-tone natural image (Figure 24)

Due to the dot-size correction capability of MECCA, continuous-tone natural images, where tonal information is known to be visually important, is reproduced with a minimum loss or shift of tonal gradation and without noticeable screening artifacts. In contrast, the visibility of a slight overdarkening due to circular-shaped print dots, leading to excessive area coverage along the envelope of clusters of dots in SUPER-CIRCLE screening, again makes the latter an inferior choice for computer-output printing of continuous-tone natural images. Note that the overdarkening effect is reduced, when using lower-resolution screens. At the same time, however, subjectively disturbing masking due to larger clusters of dots gets increased.

Independent of picture content, the subjective appearance of MECCA-processed bi-level halftone representations is far superior in quality to the one obtained with SUPER-CIRCLE screening. This improved economy of representation is achieved at the expense of increased computational complexity. While the heavy I/O traffic encountered in non-coded information-processing applications, is handled with similar overhead in MECCA and in SUPER-CIRCLE screening, the actual signal-processing tasks to be performed differ substantially from one technique to the other.

The program kernels in MECCA primarily perform *convolutions and table look-ups,* the ones in SUPER-CIRCLE screening *comparisons and cyclic rearrangements* of threshold values. In both cases, the computation time is a linear function of the number of pels processed. The execution-time ratio between MECCA and SUPER-CIRCLE screening software, implemented as PL/I programs with embedded assembler subroutines and run on various IBM/370 main-frame computers, is approximately 5:1. On a 0.8 10^6 instruction per second general-purpose computer, the average execution time for MECCA-processed pels is approximately 80 μs; a figure which can be substantially reduced using VLSI-based special-purpose low-cost processor hardware.

a)

b)

c)

d)

Figure 24. Bi-level representation of continuous-tone natural images.

a) MECCA, Q=256.
b) SUPER-CIRCLE, Q=32.
   Screening resolution: 70 clusters of dots/inch.
c) SUPER-CIRCLE, Q=64.
   Screening resolution: 47 clusters of dots/inch.
d) SUPER-CIRCLE, Q=128.
   Screening resolution: 35 clusters of dots/inch.

In order to get a better understanding of the various reproduction-quality versus computational-complexity trade-offs involved, a sufficiently *quantitative* rather than a solely *qualitative* investigation is necessary to assess the performance of MECCA and SUPER-CIRCLE screening techniques.

Contrast-Sensitivity Experiment for Performance Evaluation

In SUPER-CIRCLE screening, the quality of bi-level reproduction is limited by the fineness of the clusters of dots used. In MECCA, the quality depends on the fineness of the spatial extent over which a perceptually acceptable accuracy of the minimum average value can be reached. In general, the quality of an image reproduction process depends on its capability to reproduce spatial frequencies, and a possible solution to quantitatively evaluate its performance is to determine its modulation transfer function. The latter can be measured by generating frequency and amplitude-controlled sinusoidal gratings as shown in Figure 25.

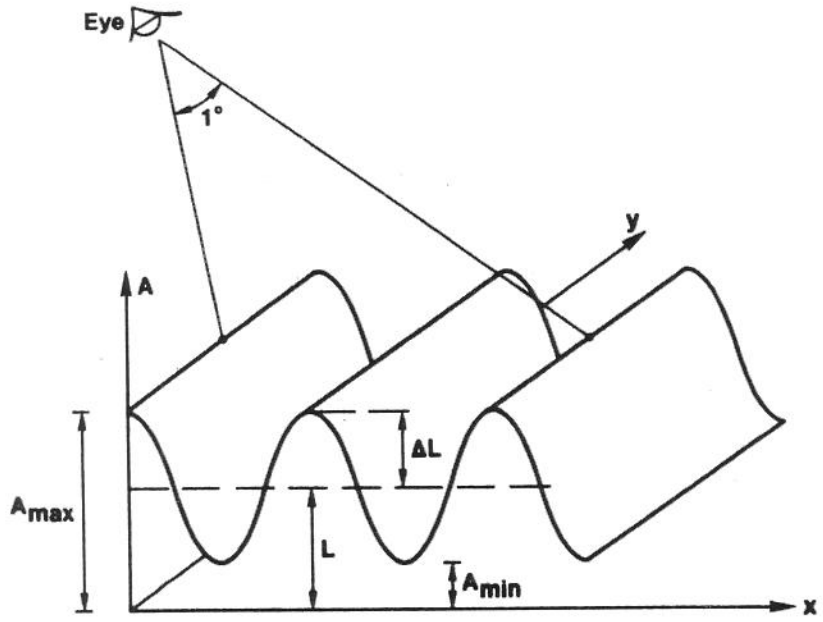

Figure 25. Parameters of sinusoidal grating.

The spatial frequency u of a grating is defined as the number of cycles that subtend an angle of one degree at the eye of its observer. The contrast or depth of modulation is defined as

$$C = (A_{max} - A_{min})/(A_{max} + A_{min}).$$

Figure 26 shows a MECCA and a SUPER-CIRCLE-processed bi-level representation of a grating in which the spatial frequency u and the reciprocal of the contrast 1/C vary logarithmically. As 1/C increases, the grating becomes more and more difficult to see until finally it appears as a uniform gray field. The intermediate zone, where the grating reaches threshold, is measurable by psychometric techniques, and its value is termed the *threshold for the perception of contrast or threshold contrast* C_T. Finally, the *contrast sensitivity* is defined as the reciprocal of C_T [10].

For more accurate measurement of the threshold contrast C_T, a large set of single spatial-frequency, single contrast-value gratings was generated using MECCA and SUPER-CIRCLE-screening techniques and reproduced on a 400 pel/inch high-resolution computer-output printing device. The 2.5 x 2.5 $inch^2$ sized hardcopy stimuli obtained were then presented, in random order, to individual observers under a viewing box that provided a high-level, constant illumination and constrained the binocular viewing distance to 12.5 inch. To determine the contrast threshold, the observers were then asked to indicate for each vertically invariant and horizontally sinusoidally varying MECCA and SUPER-CIRCLE stimulus whether, yes or no, they could see any grating. Finally, the answers obtained from 15 observers were averaged and the reciprocal plotted as the contrast sensitivity of halftoned sine-wave gratings as a function of spatial frequency (Figure 27).

The contrast-sensitivity experiment described above is based on the properties of the human eye. In order to minimize the influence of unknown non-linear effects which might arise in a psychophysical experiment involving human vision, the performance evaluation of MECCA and SUPER-CIRCLE screening is based on a comparative interpretation. The results plotted in Figure 27 show that the eye perceives peak contrast sensitivities at a spatial frequency of about 1 cycle/degree for both MECCA and SUPER-CIRCLE halftoned sine-wave gratings. Furthermore, the contrast sensitivities perceived fall off at both higher and lower spatial frequencies. However, relative to each other, the peak contrast sensitivity observed for MECCA is twice as high as for SUPER-CIRCLE screening. Similarly, cut-off is reached for MECCA at

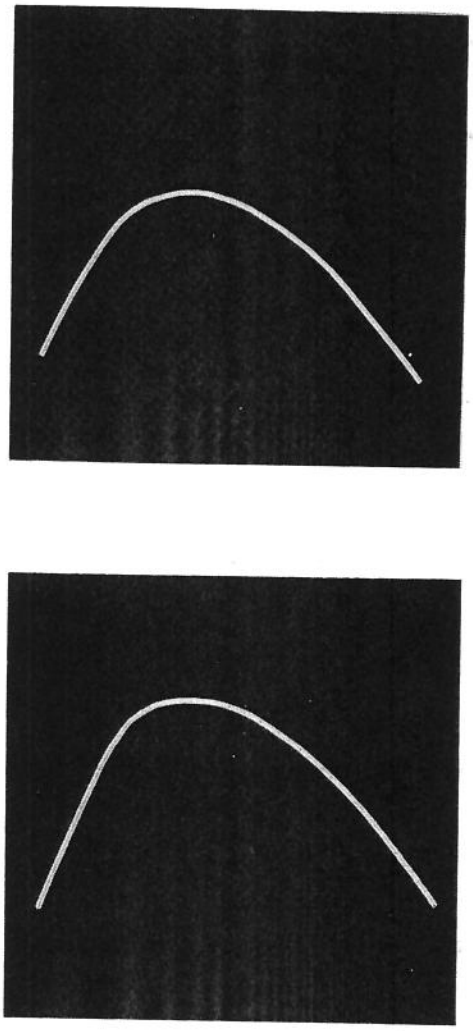

a)

b)

Figure 26. Bi-level representation of sinusoidal gratings showing the reciprocal of contrast as a function of spatial frequency.

a) SUPER-CIRCLE screening
(average gray-level set at Q/2=32).
b) MECCA
(average gray-value set at Q/2=128).

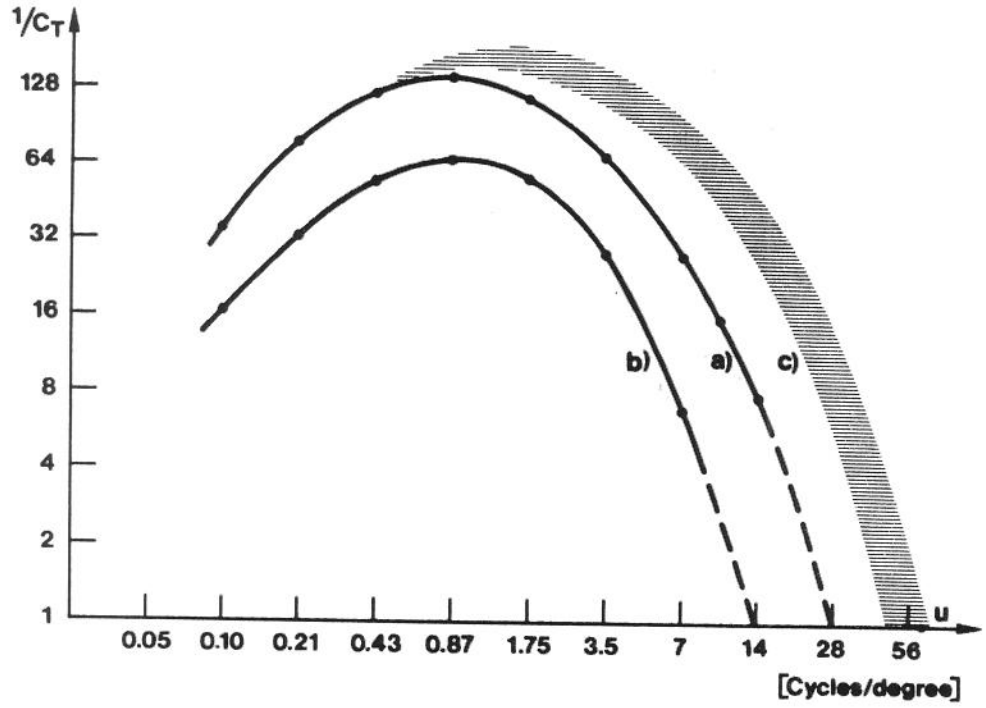

Figure 27. Observed contrast sensitivity of halftoned sine-wave gratings as a function of spatial frequency.

a) MECCA.
b) SUPER-CIRCLE screening.
c) Contrast-sensitivity domain of the human eye [10].

28 cycles/degree, a spatial frequency twice as high as for SUPER-CIRCLE screening. In order to adjust the performance of the latter to the level of MECCA, the number of reproduced dots per unit area has to be quadrupled. Consequently, the linear resolution of the computer-output printing device has to be doubled and the execution-time ratio between MECCA and SUPER-CIRCLE screening will fall to 5:4. Clearly, this is a bad engineering trade-off, since the cost of computing is constantly decreasing while the expenses for mechanical accuracy are steadily increasing.

The results plotted in Figure 27 further indicate that any spatial-frequency components that fall below threshold contrast C_T will not be observable by the average viewer and therefore need not be scanned and stored for bi-level halftone representation. For very high spatial frequencies, the threshold contrast C_T is high enough for all signals to be below this level. In practice, high spatial frequencies can be eliminated by a low enough resolution scanner or simply by low-pass filtering the scanned signal. A proper match between scanning and printing resolution also optimizes the data compression performance of continuous-tone compression schemes.

A perceptually 'perfect' bi-level halftone representation is one that ideally matches the performance of the human visual system. Figure 27 also exhibits the contrast-sensitivity domain of the human eye. Its exact limitation is difficult to indicate as it depends on many parameters such as pupil diameter, illumination and paper-reflectance conditions, etc. Without considering any technical and economic constraints, the contrast-sensitivity experiment shows that for normal viewing conditions, perceptually 'perfect' bi-level halftone representation can be achieved with MECCA and a 600 to 800 pel/inch resolution computer-output printing device.

Extensions of MECCA

The overall appearance of a bi-level image hardcopy reproduction is heavily affected by the quality of the individually printed dots. MECCA described here assumes a toner/ink deposition process capable of producing circular dots, characterized by uniform black coverage and sharp contours. Such hard dots can be achieved with various printing technologies and high-quality paper characterized by good surface smoothness and uniform ink receptivity.

For lower-quality paper or certain lower-cost printing technologies, the toner/ink deposition process tends to produce soft dots characterized by non-uniform black coverage and weak contours. In this case, the computation of the dot-size correction factor $\lambda(x,y)$ needs to be based on new design criteria.

The concept of multiple-error correction can also be extended, at the expense of increased computational complexity, to include further terms to compensate paper-specific shortcomings. For example, to neutralize the scattering of light inside dot-covered paper before it emerges, causing a slightly reduced reflectance over that expected when the internal scattering is not taken into account [11].

Application of MECCA

The concept of MECCA can be adapted to any system that incorporates all-point-addressable printers and displays of different resolution and technology. Although a detailed architectural presentation is beyond the scope of this paper, the conceptual appearance of such a system to the user can be described as follows: All stored or transmitted continuous- and halftone images are quantized for optimum image-quality rendition with an ideal reproduction device, i.e., assuming a linear relationship between the area coverage c and the amplitude quantization level q. The implementation of such a device independency concept is to add a header to each image file containing ORIGIN, DESTINATION and OUTPUT LOGICAL DEVICE attributes. If a reproduction OUTPUT LOGICAL DEVICE is specified, the image file will be put into temporary storage and automatically MECCA-processed with the set of parameters proper to the reproduction device specified. If no reproduction OUTPUT LOGICAL DEVICE is specified, the image file will be put into temporary storage and the receiver notified of its existence through higher-level functions such as data-base managers and message displays. The user can then specify the reproduction device and submit MECCA with the proper parameters.

ACKNOWLEDGMENT

The author would like to thank B. P. Medoff for early discussions on MECCA, H. Thomas and W. Butera for their treatment of dot-overlap geometries, P. Andreae for carrying out the psychophysical experiments, and C. d'Heureuse for preparing some of the halftone pictures.

APPENDIX I

Determination of $A_{overlap(x,y)}$, $A_{eff(x,y)}$ and $\lambda(x,y)$ for $L=4$

The total area of overlap at P(x,y) resulting from any combination of previously printed dots at P(x-1,y), P(x,y+1), P(x-1,y+1) and P(x+1,y+1) can be reconstructed from five component blocks F1, F2, F3, F4 and F5 as shown in Figure Ia.

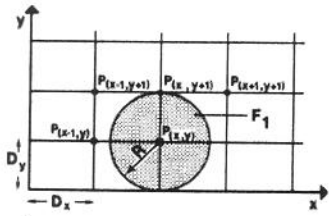

$$F_1 = \pi R^2$$

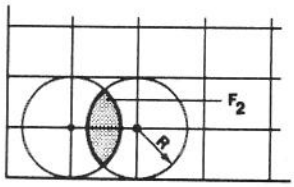

$$F_2 = 2\left[R^2\cos^{-1}\left(\frac{D_x}{2R}\right) - \frac{D_x}{2}\sqrt{R^2 - \frac{D_x^2}{4}}\right]$$

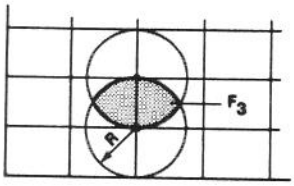

$$F_3 = 2\left[R^2\cos^{-1}\left(\frac{D_y}{2R}\right) - \frac{D_y}{2}\sqrt{R^2 - \frac{D_y^2}{4}}\right]$$

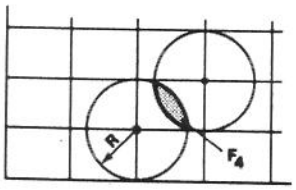

$$F_4 = 2\left[R^2\cos^{-1}\left(\frac{\sqrt{D_x^2+D_y^2}}{2R}\right) - \frac{\sqrt{D_x^2+D_y^2}}{2}\sqrt{R^2 - \frac{D_x^2+D_y^2}{4}}\right]$$

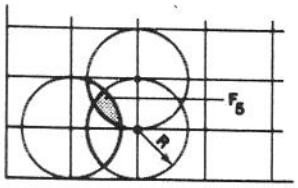

$$F_5 = 0.5\left((D_x \cdot D_y) + F_2 + F_3 + F_4 - F_1\right)$$

Figure Ia. The five component blocks to compute the area of overlap.

An example demonstrating the computation of $A_{overlap}(x,y)$ is shown in Figure Ib.

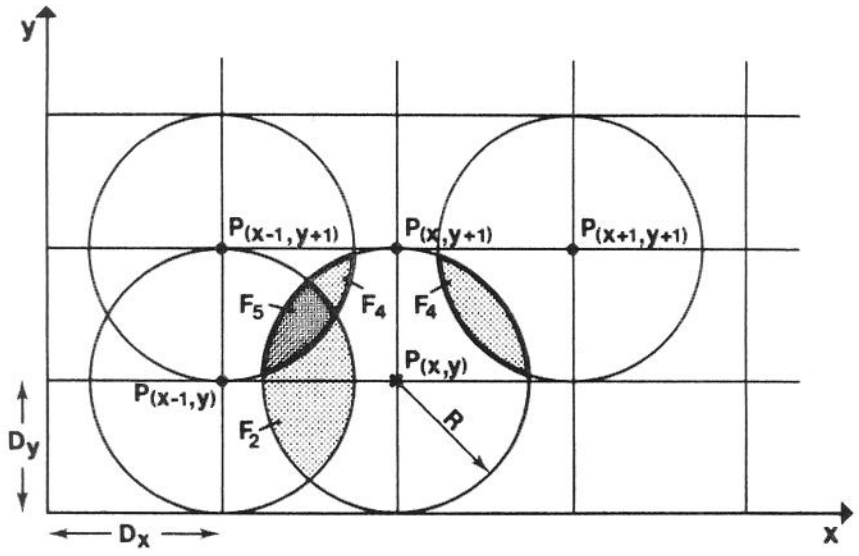

Figure Ib. Example of overlap computation using component blocks.

For given parameters D_x, D_y and R, the overlap between the circles centered at P(x,y) and P(x+1,y+1) is given by F4. The overlap between the circles centered at P(x,y) and P(x-1,y+1) is also described by F4. The area common to the circles centered at P(x,y) and P(x-1,y) is given by F2. Finally, the common area between three mutually adjacent dots centered at P(x,y), P(x-1,y) and P(x-1,y+1) is described by F5. The total area of overlap therefore amounts to

$$A_{overlap}(x,y) = F2 + 2F4 - F5.$$

The effective area of white paper newly covered is

$$A_{eff}(x,y) = F1 - A_{overlap}(x,y),$$

and the dot-size correction value

$$\lambda(x,y) = A_{eff}(x,y)/(D_x\ D_y).$$

Table I lists all possible overlap combinations for L=4 adjacent print positions and the corresponding formulas to compute $A_{eff}(x,y)$.

P(x+1,y+1)	P(x,y+1)	P(x-1,y+1)	P(x-1,y)	$A_{eff}(x,y)$
0	0	0	0	F1
0	0	0	1	F1 - F2
0	0	1	0	F1 - F4
0	0	1	1	F1 - F2 - F4 + F5
0	1	0	0	F1 - F3
0	1	0	1	F1 - F2 - F3 + F5
0	1	1	0	F1 - F3 - F4 + F5
0	1	1	1	F1 - F2 - F3 + F5
1	0	0	0	F1 - F4
1	0	0	1	F1 - F4 - F2
1	0	1	0	F1 - 2F4
1	0	1	1	F1 - F2 - 2F4 + F5
1	1	0	0	F1 - F3 - F4 + F5
1	1	0	1	F1 - F2 - F3 - F4 + 2F5
1	1	1	0	F1 - F3 - 2F4 + 2F5
1	1	1	1	F1 - F2 - F3 - F4 + 2F5

('1' = dot, '0' = no dot)

Table I. All possible overlap contributions for L=4 adjacent print positions and the corresponding expressions for $A_{eff}(x,y)$.

APPENDIX II

Determination of $A_{overlap}(x,y)$, $A_{eff}(x,y)$ and $\lambda(x,y)$ for L=6

The total area of overlap at P(x,y) resulting from any combination of previously printed dots at P(x-1,y), P(x,y+1), P(x-1,y+1), P(x+1,y+1), P(x-2,y) and P(x,y+2) can be reconstructed using the technique of component blocks. For L=6 dots, nine component blocks are necessary to reconstruct the total overlap for a given printed dot configuration. Five of these blocks are the same as the ones used in the L=4 dot case, while the remaining four blocks are unique to the L=6 dot case (Figure IIa).

An example involving L=6 potentially overlaping neighbor dots is shown in Figure IIb. Here, the dots centered at print positions P(x-1,y+1), P(x,y+1) and P(x-2,y) are already present when the dot centered at P(x,y) is printed.

In order to compute the total overlap area $A_{overlap}(x,y)$, the contribution from each printed neighboring dot is considered and adjustments are made to ensure that no part of an overlap is counted more than once. For the case shown in Figure IIb,

$$A_{eff}(x,y) = F1 - A_{overlap}(x,y) = F1 - [F3 + (F4 - F5) + (F6 - F8)],$$

where

- F1 : Area of circular dot,
- F3 : Overlap between dot centered at P(x,y) and dot centered at P(x,y+1),
- F4 : Overlap between dot centered at P(x,y) and dot centered at P(x-1,y+1),
- F5 : Correction value used to keep the area common to dots centered at P(x,y+1), P(x-1,y+1) and P(x,y) from being counted twice,
- F6 : Overlap between dot centered at P(x,y) and dot centered at P(x-2,y),
- F8 : Correction value used to keep the area common to dots centered at P(x-1,y+1), P(x-2,y) and P(x,y) from being counted twice.

Table II lists all possible overlap combinations for L=6 adjacent print positions and the corresponding formulas to compute $A_{eff}(x,y)$.

P(x,y+2)	P(x-2,y)	P(x+1,y+1)	P(x,y+1)	P(x-1,y+1)	P(x-1,y)	$A_{eff}(x,y)$
0	0	0	0	0	0	F1
0	0	0	0	0	1	F1 - F2
0	0	0	0	1	0	F1 - F4
0	0	0	0	1	1	F1 - F2 - F4 + F5
0	0	0	1	0	0	F1 - F3
0	0	0	1	0	1	F1 - F2 - F3 + F5
0	0	0	1	1	0	F1 - F3 - F4 + F5
0	0	0	1	1	1	F1 - F2 - F3 + F5
0	0	1	0	0	0	F1 - F4
0	0	1	0	0	1	F1 - F4 - F2
0	0	1	0	1	0	F1 - 2F4 + F8
0	0	1	0	1	1	F1 - F2 - 2F4 + F5 + F8
0	0	1	1	0	0	F1 - F4 - F3 + F5
0	0	1	1	0	1	F1 - F4 - F3 - F2 + 2F5
0	0	1	1	1	0	F1 - 2F4 - F3 + 2F5
0	0	1	1	1	1	F1 - F4 - F3 - F2 + 2F5
0	1	0	0	0	0	F1 - F6
0	1	0	0	0	1	F1 - F2
0	1	0	0	1	0	F1 - F6 - F4 + F8
0	1	0	0	1	1	F1 - F2 - F4 + F5
0	1	0	1	0	0	F1 - F6 - F3
0	1	0	1	0	1	F1 - F2 - F3 + F5
0	1	0	1	1	0	F1 - F3 - F4 + F5 + F8 - F6
0	1	0	1	1	1	F1 - F2 - F3 - F5
0	1	1	0	0	0	F1 - F6 - F4
0	1	1	0	0	1	F1 - F4 - F2
0	1	1	0	1	0	F1 - F6 - F4 + F8 - F4 + F8
0	1	1	0	1	1	F1 - F2 - 2F4 + F5 + F8
0	1	1	1	0	0	F1 - F6 - F3 - F4 + F5
0	1	1	1	0	1	F1 - F4 - F3 - F2 + 2F5
0	1	1	1	1	0	F1 - F6 - F4 + F8 - F3 - F4 + 2F5
0	1	1	1	1	1	F1 - F4 - F3 - F2 + 2F5
1	0	0	0	0	0	F1 - F7
1	0	0	0	0	1	F1 - F2 - F7
1	0	0	0	1	0	F1 - F4 - F7 + F9
1	0	0	0	1	1	F1 - F2 - F4 + F5 - F7 + F9
1	0	0	1	0	0	F1 - F3
1	0	0	1	0	1	F1 - F2 - F3 + F5
1	0	0	1	1	0	F1 - F3 - F4 + F5
1	0	0	1	1	1	F1 - F2 - F3 + F5
1	0	1	0	0	0	F1 - F4 - F7 + F9
1	0	1	0	0	1	F1 - F2 - F4 - F7 + F9
1	0	1	0	1	0	F1 - 2F4 + F8
1	0	1	0	1	1	F1 - F2 - 2F4 + F5 + F8
1	0	1	1	0	0	F1 - F4 - F3 + F5
1	0	1	1	0	1	F1 - F4 - F3 - F2 + 2F5
1	0	1	1	1	0	F1 - 2F4 - F3 + 2F5
1	0	1	1	1	1	F1 - F4 - F3 - F2 + 2F5
1	1	0	0	0	0	F1 - F6 - F7
1	1	0	0	0	1	F1 - F2 - F7
1	1	0	0	1	0	F1 - F7 - F6 - F4 + F8 + F9
1	1	0	0	1	1	F1 - F2 - F4 + F5 - F7 + F9
1	1	0	1	0	0	F1 - F6 - F3
1	1	0	1	0	1	F1 - F2 - F3 + F5
1	1	0	1	1	0	F1 - F3 - F4 + F5 + F8 - F6
1	1	0	1	1	1	F1 - F2 - F3 + F5
1	1	1	0	0	0	F1 - F4 - F7 + F9 - F6
1	1	1	0	0	1	F1 - F2 - F4 - F7 + F9
1	1	1	0	1	0	F1 - F6 - F4 + F8 - F4 + F8
1	1	1	0	1	1	F1 - F2 - 2F4 + F5 + F8
1	1	1	1	0	0	F1 - F6 - F3 - F4 + F5
1	1	1	1	0	1	F1 - F4 - F3 - F2 + 2F5
1	1	1	1	1	0	F1 - F6 - 2F4 + F8 - F3 + 2F5
1	1	1	1	1	1	F1 - F4 - F3 - F2 + 2F5

('1' = dot, '0' = no dot)

Table II. All possible overlap contributions for L=6 adjacent print positions and the corresponding expresions for $A_{eff}(x,y)$.

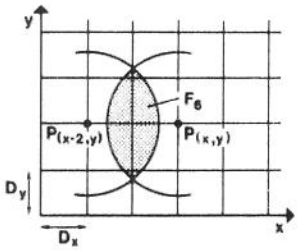

$$F_6 = 2\left[R^2\cos^{-1}\left(\frac{D_x}{2}\right) - D_x\sqrt{R^2 - D_x^2}\right]$$

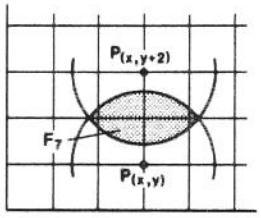

$$F_7 = 2\left[R^2\cos^{-1}\left(\frac{D_y}{2}\right) - D_y\sqrt{R^2 - D_y^2}\right]$$

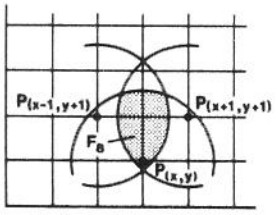

$$F_8 = F_6/2 + F_4 - F_1/2 + (D_x \cdot D_y)$$

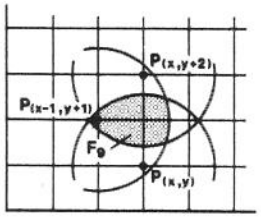

$$F_9 = F_7/2 + F_4 - F_1/2 + (D_x \cdot D_y)$$

Figure IIa. The four component blocks unique to the L=6 dot case.

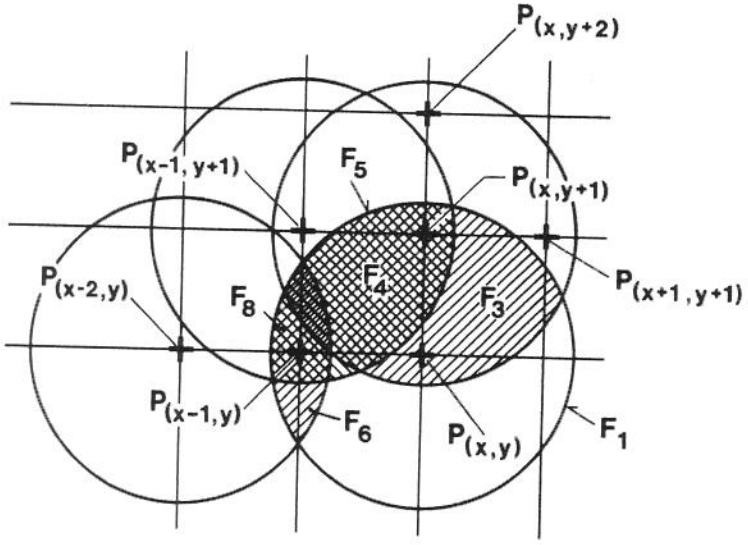

Figure IIb. Example involving L=6 potentially overlaping neighbor dots.

REFERENCES

[1] P. Stucki, 'Statistical Measurements for Television Picture Classification and Some Experiments in Video Signal Encoding', DIC Thesis, Imperial College of Science and Technology, London, July 1968.

[2] J. O. Limb, 'Design of Dither Waveforms for Quantized Visual Signals', Bell Syst. Tech. J., Vol. 48, No. 7, 1969.

[3] B. E. Bayer, 'An Optimum Method for Two-Level Rendition of Continuous-Tone Pictures', International Conference on Communications, Conference Record, CAT. No. 73 CHO 744-3CSCB, June 1973.

[4] P. Stucki, 'Comparison and Optimization of Computer-Generated Digital Halftone Pictures', SID Digest of Technical Papers, Vol. VI, 1975.

[5] G. C. Higgins and K. Stultz, 'Visual Acuity as Measured with Various Orientations of a Parallel-Line Test Object', J. Opt. Soc. Am., Vol. 38, No. 9, 1948.

[6] P. Stucki, 'Image Processing for Document Reproduction' in *Advances in Digital Image Processing*, P. Stucki, Ed., Plenum Presss, NY, 1979.

[7] K. Y. Wong and P. Stucki, 'Adaptive Switching of Dispersed and Clustered Dot Patterns for Bi-Level Halftone Rendition', SID Digest of Technical Papers, Vol. VIII, 1977.

[8] R. Floyd, 'An Adaptive Algorithm for Spatial Gray-Scale', SID Digest of Technical Papers, Vol. VI, 1975.

[9] J. F. Jarvis, C. N. Judice and W. H. Ninke, 'A Survey of Techniques for the Display of Continuous-Tone Pictures on Bilevel Displays', Computer Graphics and Image Processing, Vol. 5, No. 7, 1976.

[10] F. W. Campbell, 'The Human Eye as an Optical Filter', Proc. IEEE, Vol. 56, No. 6, 1968.

[11] F. R. Clapper and J. A. C. Yule, 'The Effect of Multiple Internal Reflections on the Densities of Half-Tone Prints on Paper', J. Opt. Soc. Am., Vol. 43, No. 7, 1953.